ACS APPLIED MATERIALS & INTERFACES

Research Article

www.acsami.org

Silver Nanoparticles and Growth Factors Incorporated Hydroxyapatite Coatings on Metallic Implant Surfaces for Enhancement of Osteoinductivity and Antibacterial Properties

Chao-Ming Xie,[†] Xiong Lu,*[,†] Ke-Feng Wang,[‡] Fan-Zhi Meng,[§] Ou Jiang,[§] Hong-Ping Zhang,[∥] Wei Zhi,[†] and Li-Ming Fang[⊥]

[†]Key Lab of Advanced Technologies of Materials, Ministry of Education, School of Materials Science and Engineering, Southwest Jiaotong University, Chengdu, Sichuan 610031, China

[‡]National Engineering Research Center for Biomaterials, Sichuan University, Chengdu, Sichuan 610064, China

[§]The Second People's Hospital of Neijiang, Neijiang, Sichuan 641000, China

[∥]School of Materials Science and Engineering, Southwest University of Science and Technology, Mianyang, Sichuan 621000, China

[⊥]School of Materials Science and Engineering, South China University of Technology, Guangzhou 510641, China

Supporting Information

ABSTRACT: Research on incorporation of both growth factors and silver (Ag) into hydroxyapatite (HA) coatings on metallic implant surfaces for enhancing osteoinductivity and antibacterial properties is a challenging work. Generally, Ag nanoparticles are easy to agglomerate and lead to a large increase in local Ag concentration, which could potentially affect cell activity. On the other hand, growth factors immobilization requires mild processing conditions so as to maintain their activities. In this study, bone morphology protein-2 (BMP-2) and Ag nanoparticle contained HA coatings were prepared on Ti surfaces by combining electrochemical deposition (ED) of Ag and electrostatic immobilization of BMP-2. During the ED process, chitosan (CS) was selected as the stabilizing agent to chelate Ag ions and generate Ag nanoparticles that are uniformly distributed in the coatings. CS also reduces Ag toxicity while retaining its antibacterial activity. Afterwards, a BMP/heparin solution was absorbed on the CS/Ag/HA coatings. Consequently, BMP-2 was immobilized on the coatings by the electrostatic attraction between CS, heparin, and BMP-2. Sustained release of BMP-2 and Ag ions from HA coatings was successfully demonstrated for a long period. Results of antibacterial tests indicate that the CS/Ag/HA coatings have high antibacterial properties against both *Staphylococcus epidermidis* and *Escherichia coli*. Osteoblasts (OB) culture reveals that the CS/Ag/HA coatings exhibit good biocompatibility. Bone marrow stromal cells (BMSCs) culture indicates that the BMP/CS/Ag/HA coatings have good osteoinductivity and promote the differentiation of BMSCs. Ti bars with BMP/CS/Ag/HA coatings were implanted into the femur of rabbits to evaluate the osteoinductivity of the coatings. Results indicate that BMP/CS/Ag/HA coatings favor bone formation in vivo. In summary, this study presents a convenient and effective method for the incorporation of growth factors and antibacterial agents into HA coatings. This method can be utilized to modify a variety of metallic implant surfaces.

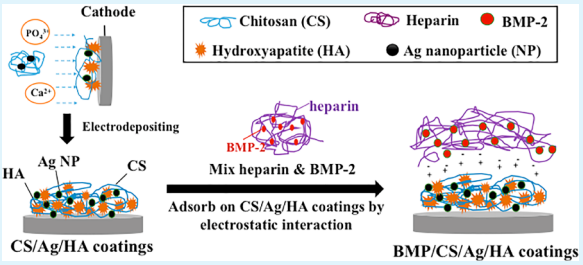

KEYWORDS: *hydroxyapatite coating, BMP-2, silver nanoparticle, dual release, osteoinductivity, antibacterial property*

1. INTRODUCTION

Over the past decades, medical metallic implants have been widely used in orthopedic and dental applications. However, metallic implants are biologically inert and cannot induce bone regeneration after implantation. One approach to improve the osteoinducivity of metallic implants is to deposit calcium phosphates (CaP) coatings on surfaces.[1,2] CaP coatings are known to have good biological performance and enhance fixation and long-term survival of metallic implants.[3] Moreover, CaP can also be used for delivery of growth factors for bone repair.[4,5] Bone morphogenetic protein-2 (BMP-2) is one of the most important growth factors that can induce bone formation by causing the migration of mesenchymal stem cells and their differentiation into osteoblasts.[6−8] CaP coatings incorporated with BMP-2 could further improve the osteoinductivity of implants. Incorporation of BMP-2 into CaP coatings can be done in two ways, namely, physical adsorption and chemical fixation. Physical absorption, which involves adsorption of BMP-2 on the CaP coatings, generally cause early burst release of BMP, which could not result in good long-term therapy.[9,10] Chemical fixation through covalent binding of BMP-2 on carboxylated CaP coatings could facilitate relatively long term

Received: March 10, 2014
Accepted: April 10, 2014
Published: April 10, 2014

release.[11] However, chemical fixation could exert detrimental effects on the stability and activity of BMP-2.[12]

CaP coatings could also promote bacterial adhesion together with their osteoinductivity,[13,14] and can eventually lead to a second surgery.[15,16] This challenge could be addressed by release of antibacterial agents from the CaP coatings.[4] Antibiotics are mostly used as antibacterial agents to treat various bacterial infections, but the risk of antibiotic resistance has increasingly become a major concern.[17] Silver (Ag) exhibits potent antibacterial activity against a number of Gram-positive and Gram-negative bacteria, and bacterial resistance against silver is minimal.[18] Incorporation of Ag nanoparticles (NP) into CaP coatings is effective in providing long-term antibacterial properties to CaP coatings. Various methods have been employed to incorporate Ag into CaP coatings, such as plasma spraying,[19,20] ion beam assisted deposition,[21] and magnetron sputtering.[22] However, these methods are line-of-sight technologies that cannot be applied to the medical devices with complex shapes. Micro-arc oxidation[23] and sol−gel technology[24,25] have also been used to prepare Ag-containing CaP coatings. Notably, Ag NPs are easy to agglomerate and easily lead to a large increase in local Ag concentration, which could potentially affect cell activity. Thus, the uniform distribution of Ag NPs is critical for the success of Ag-containing CaP coatings.[26]

In the present study, hydroxyapatite (HA) coatings that are capable of dual release of Ag ions and BMP-2 were prepared. The CaP coatings were co-deposited with CS and Ag on Ti surfaces by electrochemical deposition (ED), a mild method that can be used to prepare Ag-containing HA coatings on metallic implants with complex geometries.[27] BMP-2 was immobilized by adsorbing BMP/heparin mixed solutions on CS/Ag/HA coatings, as shown in Scheme 1. The morphologies, release kinetics of BMP-2 and Ag, antibacterial activity, and biocompatibility of the coatings were evaluated. The osteoinductivity of BMP/CS/Ag/HA coatings was investigated in vitro and in vivo.

Scheme 1. Schematic of the Electrochemical Deposition Process and Immobilization of BMP-2 on HA Coatings[a]

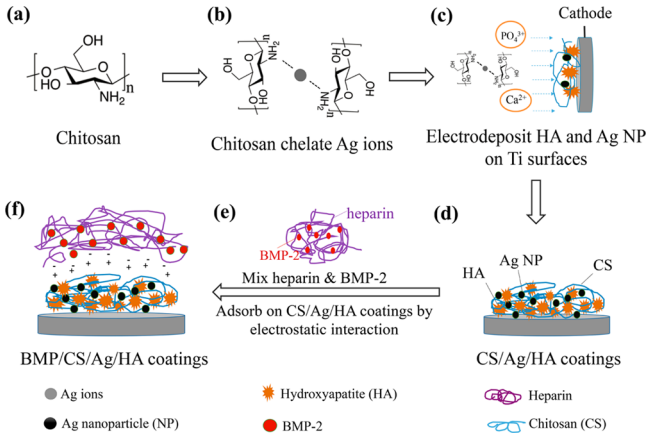

[a](a) Structure of chitosan. (b) Chitosan chelate Ag ions in the electrolytes. (c) CS/Ag/HA coatings are prepared by co-electrodeposition of CS-Ag^{+}, Ca^{2+}, and PO_4^{3+} on Ti surfaces. (d) CS/Ag/HA coatings are formed. (e) BMP-2 and heparin are mixed. (f) BMP/CS/Ag/HA coatings are formed by adsorbing BMP-2/heparin mixed solution on CS/Ag/HA coatings. BMP-2 is immobilized through electrostatic interaction.

2. MATERIALS AND METHODS

2.1. Pretreatment of Ti Specimens. First, commercially pure Ti (Bao Ji Special Iron and Steel Co. Ltd, China) was cut into discs with diameters of 8 mm and then mechanically polished using a series of SiC papers (240, 400, and 800 grit). Second, the discs were etched in a mixed acid (H_2SO_4/HCl/H_2O = 1:1:1, volume ratio) at 60 °C for 3 h to remove natural oxide layers and increase surface roughness. Third, the discs were alkali-treated to increase the hydrophilicity by immersion in 100 mL of 5 M NaOH aqueous solution at 60 °C for 3 h. The Ti discs are referred to as pristine Ti in subsequent sections.

2.2. Preparation of CS/Ag/HA Coatings. CS/Ag/HA, Ag/HA, and pure HA coatings were prepared by pulsed ED,[27] which was conducted in the cell consisting of the following three electrodes: the Ti discs as working electrode, a Pt plate as the counter electrode, and a saturated calomel electrode as the reference electrode. The ED was carried out with a pulse width of 100 s for 1 h at −1.3 V. The electrolyte of CS/Ag/HA coatings was an aqueous solution containing 5 mM $Ca(NO_3)_2$, 3 mM $NH_4H_2PO_4$, 0.05 g/L $AgNO_3$, and 0.22 g/L CS (low molecular weight, Sigma). The pH value of electrolytes was adjusted to 5.0 using ammonia. The electrolyte used for the Ag/HA coatings was the same as that used for CS/Ag/HA coatings without CS. Pure HA coatings were also prepared by pulsed ED, which was conducted with a pulse width of 100 s for 1 h at −1.5 V. The electrolyte was an aqueous solution of 10 mM $Ca(NO_3)_2$ and 6 mM $NH_4H_2PO_4$. After deposition, the coated Ti discs were rinsed with deionized water and subsequently dried in air.

2.3. Loading BMP-2 on the Composite Coatings. BMP-2/heparin mixed solution was prepared by dissolving BMP-2 (Rebone, China) and heparin in phosphate buffer solution (PBS). The concentration of BMP-2 in the solution is 5 μg/mL. Afterward, 50 μL of BMP-2/heparin mixed solution was dropped on the CS/Ag/HA and Ag/HA coatings to obtain BMP/CS/Ag/HA and BMP/Ag/HA coatings, respectively. Each coating contained 0.25 μg of BMP-2. The coatings were dried overnight at room temperature.

2.4. Characterization of Coatings. A scanning electron microscope (SEM; JSM 6390, JEOL, Japan) equipped with an X-ray energy dispersive spectrometer (EDS) was used to examine the morphology and composition of the CS/Ag/HA, Ag/HA and pure HA coatings. A transmission electron microscope (TEM; JEOL 2010, JEOL, Japan) was used to investigate the microstructures of the HA and Ag extracted from CS/Ag/HA-Ti surfaces. An X-ray diffractometer (XRD; X'pert PRO, Philips, The Netherlands) was used to identify the crystalline phases of the coatings. Fourier transform infrared spectroscopy (FT-IR; Nicolet 5700, Thermo) was used to determine the chemical composition of the deposited coatings. Thermogravimetric (TG; Netzsch TG 209 F1, Germany) analysis was performed to determine the mass ratio of the coatings from 20 to 800 °C at a rate of 10 °C/min. The adhesive strengths of the coatings were measured using a universal testing machine (Instron 5567). The adhesion strength was calculated as the load at failure divided by the area of samples. The data were the average of six samples.

2.5. Ag Release and Antibacterial Tests. BMP/CS/Ag/HA, CS/Ag/HA, and Ag/HA coatings were soaked in 5 mL of PBS at varying time periods (1, 3, 5, 10, 15, 20, 25, and 31 days) to examine Ag release. Three parallel samples of each group were used for the Ag release test. At each time interval, the solution was collected and replaced with 5 mL of fresh PBS. The Ag concentration of the collected solution was measured using an atomic absorption spectrophotometer (AAS; Z-2300, Hitachi, Japan). *Staphylococcus epidermidis* (ATCC 12228) and *Escherichia coli* (ATCC 8739) were used to evaluate the antibacterial activity of the coatings. During antibacterial tests, BMP/CS/Ag/HA, CS/Ag/HA, and Ag/HA coatings were selected as the experimental groups, and pristine Ti was selected as the contrastive group. Four parallel samples of each group were used for the antibacterial test. All bacteria were cultured in Luria-Bertani (LB) broth. First, the samples were placed in a 24-well plate, and 100 μL of bacterial suspension (10^6 CFU/mL) was added onto the surfaces of each sample. Next, the samples were incubated for 12 h at 37°C in an incubator. Afterward, 900 mL of LB broth was added to

dx.doi.org/10.1021/am501428e | ACS Appl. Mater. Interfaces 2014, 6, 8580−8589

each well in the plates, and the samples were further incubated for 12 h at 37 °C. Finally, 200 μL of bacterial suspension on each sample was collected and transferred to a 96-well plate. Bacterial growth was monitored by measuring optical density (OD) at 600 nm in a microplate reader (MQX200, BioTEK). The bactericidal ratio of the coatings was calculated according to the following equation:[28,29]

$$\text{bactericidal ratio (\%)} = \frac{\text{OD of contrastive group} - \text{OD of experimental group}}{\text{OD of contrasive group}} \times 100\% \quad (1)$$

2.6. In Vitro BMP-2 Release. The BMP/CS/Ag/HA and BMP/Ag/HA were incubated in 1 mL of PBS to evaluate the release kinetics of BMP-2 immobilized on CaP coatings. Incubation was carried out with shaking at 37°C. At the time intervals of 1, 3, 5, 7, 10, 13, 18, and 25 days, the solution was collected and replaced with fresh solution. The BMP-2 concentration of the collected solution was determined using a human BMP-2 ELISA Kit (R&D).

2.7. Culture of Osteoblasts. Osteoblasts (OB; MC3T3-E1, CRL-2593, ATCC) were cultured on various coatings to evaluate the biocompatibility of the samples. The following four groups of samples were used: CS/Ag/HA, Ag/HA, pure HA, and pristine Ti. OB were cultured in α-MEM (HyClone) supplemented with 10% fetal bovine serum (FBS; HyClone) and 1% penicillin−streptomycin solution (HyClone). The cell density was 2×10^4 cells/sample. The culture medium was replaced every 2 days.

Cell morphology was observed using the SEM (JSM 6390) after 3 and 7 days of culture. First, the medium was removed and the cells were fixed in a solution containing 2.5% glutaraldehyde for 4 h. Second, the cells were dehydrated through a graded series of alcohol, and then dealcoholized by immersing in a graded series of ethyl acetate. Finally, cells were critically point dried and gold-sputtered prior to SEM observation.

Cell proliferation was evaluated by the Alamar Blue assay after 3 and 7 days of culture. During the Alamar Blue assay, the culture medium in the 24-well plate was replaced with 300 μL of Medium 199 (GIBCO) supplemented with 10% FBS and 10% Alamar Blue. The cells were incubated at standard cell culture conditions for 4 h. The OD of the medium was read at 600 and 570 nm against a medium-blank Alamar Blue in a microplate reader (MQX200).

The differentiation of cells was evaluated by the ALP activity assay. After 7 days of culture, the medium was removed from the wells and the cells were washed twice with PBS. Afterward, 300 μL of 1 % Triton X-100 (Amresco) was used to lyse the cells in each well. The total protein concentration of the cell lysate of each sample was measured using a BCA Kit (Jiancheng Biotech, China). ALP activity was measured using an ALP Assay Kit (Jiancheng Biotech). The final ALP activity was normalized with respect to the total protein content obtained from the same cell lysate. In each case, four specimens were tested and the assay was repeated two times.

2.8. Culture of BMSCs. BMSCs were cultured on various coatings to evaluate the osteoinductivity of the coatings. The following four groups of samples were used: BMP/CS/Ag/HA, CS/Ag/HA, BMP/Ag/HA, pure HA, and pristine Ti. BMSCs were extracted from 1 week old SD rats. After purification and passage, BMSCs were seeded on four groups of samples with the density of 5×10^4 cells/sample. The culture medium was α-MEM supplemented with 10% FBS and 1% penicillin−streptomycin solution. The morphologies of BMSCs were assessed using immunofluorescence staining. After fixation, cells were incubated in blocking solution (10 mg/mL of bovine serum albumin) for 30 min at room temperature. The cells were then incubated with primary antibody anti-actin (BIOTER, China), second antibody goat-anti-rabbit (BIOTER), and Rabbit Anti-Goat IgG-TRITC (BIOTER). Finally, cells were mounted with glycerol, and observed under a fluorescent microscope (DMIL, Leica, Germany). Cell proliferation was evaluated using the Alamar Blue assay at 3 and 7 days. The differentiation of cells was evaluated using the ALP activity assay after 14 days of culture. The details of the test methods are described in Section 2.7.

2.9. Animal Experiments. Ti bars (Φ 2 × 5 mm) with BMP/CS/Ag/HA coatings, and BMP/Ag/HA coatings were implanted into the femurs of rabbits to evaluate the osteoconductivity of the coatings in vivo. The experiments were performed in accordance with protocols approved by the local ethical committee and laboratory animal administration rules of China. Four Japanese big-ear white rabbits with a mean body weight of 3 kg were used. Surgery was performed under conditions of general anesthesia with 2% pentobarbital sodium. The Ti bars were placed in the 3 mm holes on the thighbone, which were pre-opened using a bone drill, on one hind leg of each rabbit (Supporting Information Figure S1). After surgery, the rabbits were administered with penicillin for 3 days.

All rabbits were sacrificed through air embolism after 12 weeks. The specimens were fixed for histological observations. First, the specimens were fixed in 10% formalin in 0.01 M PBS for 7 days at 4 °C, rinsed in water for 24 h, dehydrated with gradient concentrations of alcohol, infiltrated with xylene, and embedded in PMMA polymerized from MMA. Second, PMMA fixed specimens were cut into 200 μm thin sections using a Lecia 1600 slicer (Microm, France). Finally, thin sections were stained with Van Gieson to detect the new bone formation. The stained sections were observed with a light microscope (Olympus 60X, Japan). The retrieved specimens were also scanned with a Micro-CT scanner (XTV160H; X-TEK, England) to observe the new bone formation around the specimens. The scanning was performed at 90 kV and 40 μA.

2.10. Statistical Analysis. The data were analyzed by one-way analysis of variance (ANOVA) followed by Tukey's multiple-comparison post hoc test to determine any statistical significance of difference between the test groups. The level of statistical significance was set at $p \leq 0.05$.

3. RESULTS

3.1. Characterizations of CS/Ag/HA Coatings. The SEM micrograph in Figure 1a reveals that Ag NPs are uniformly

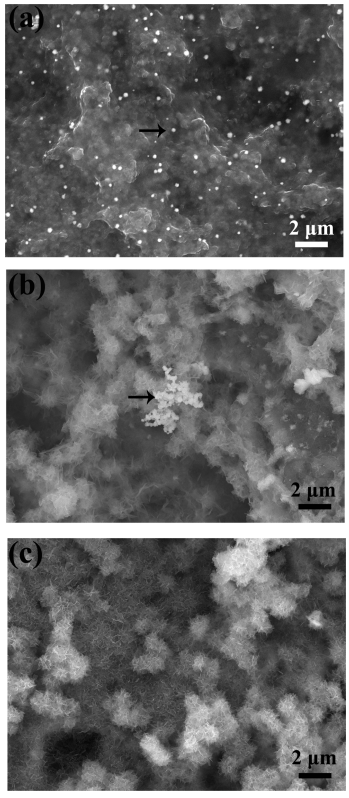

Figure 1. SEM micrographs of (a) CS/Ag/HA coatings, (b) Ag/HA coatings, and (c) HA coatings.

distributed in CS/Ag/HA coatings, and the sizes of Ag NP range from 100 to 200 nm. In Ag/HA coatings, Ag NPs agglomerate and forms large clusters (Figure 1b). The HA in the Ag/HA coatings and pure HA coatings have flowerlike structures (Figure 1b and c). However, HA in CS/Ag/HA coatings does not exhibit the typical morphology because it is covered by CS molecules (Figure 1a). The cross-sectional view of the CS/Ag/HA coating indicates that thickness of the coating is about 20 μm. EDS line scanning was conducted through the cross section of coatings, which proves that Ag is distributed inside the CS/Ag/HA coatings (Figure 2). To

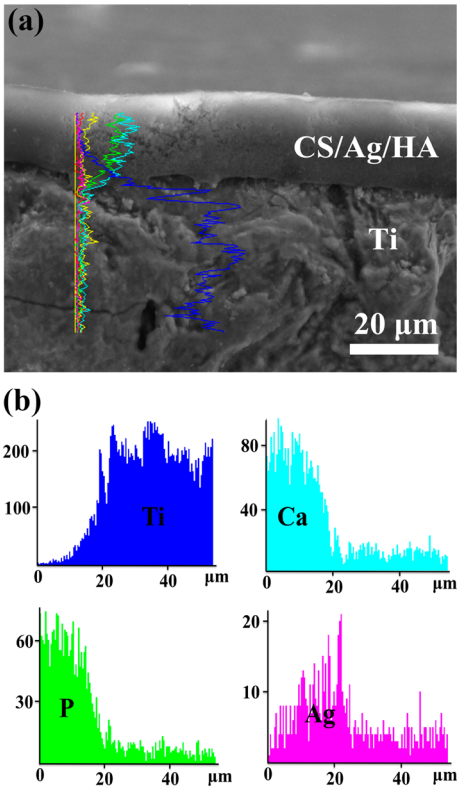

Figure 2. (a) EDS line scanning along the cross section of CS/Ag/HA coatings. (b) Elemental distribution along the EDS line.

determine the composition of the coatings, EDS detection was performed on the different area of three parallel samples. The results reveal that the atomic ratios of Ca to P in CS/Ag/HA and Ag/HA are 1.60 and 1.45, which is close to the atomic ratio of HA. The TEM micrograph in Figure 3a also demonstrates that Ag NP uniformly distributes in the coatings that are extracted from Ti specimen surfaces. The high-resolution TEM (HRTEM) micrograph in Figure 3b shows that the lattice fringe of crystalline HA appears around the Ag NP, which indicates that Ag NP and crystalline HA integrate seamlessly. The thin film X-ray diffraction (TF-XRD) spectra of the CS/Ag/HA and Ag/HA coatings exhibit typical HA peaks at 2θ value of 25.8° and in the range of 31.7−33° (Figure 4). TF-XRD spectra also show that the CS/Ag/HA and Ag/HA coatings contain well-crystallized Ag, as revealed by the diffraction peaks at 2θ values of 38° and 44.3° that are corresponding to the (1 1 1) and (2 0 0) planes of Ag, respectively. In the FT-IR spectrum of CS/Ag/HA coating (Supporting Information Figure S2), the peaks at 3444 and 1646 cm^{-1} belong to the amide group of CS, which confirms

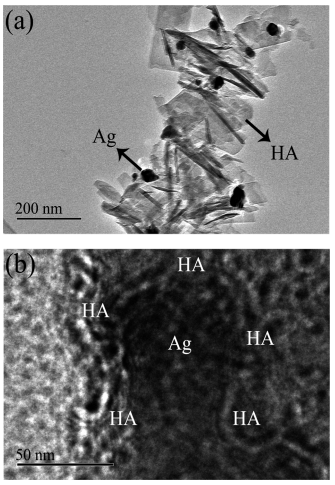

Figure 3. (a) TEM micrograph of the CS/Ag/HA coatings extracted from Ti surfaces. (b) HRTEM micrograph of the CS/Ag/HA coatings.

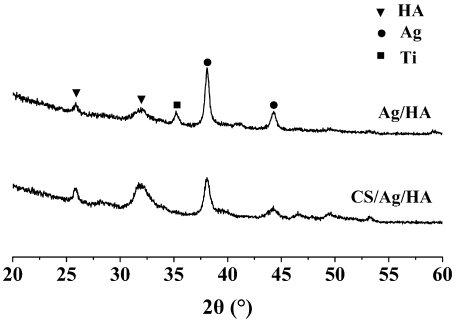

Figure 4. TF-XRD spectra of CS/Ag/HA and Ag/HA coatings.

the presence of CS in the coatings. FT-IR characterization further proves the success of the ED process. The TG analysis results reveal that the weight percentage of CS in CS/Ag/HA coatings was 15.7 wt % (Supporting Information Figure S3). Note that, from EDS results, the mass ratio of HA to Ag is 19.5 wt %. Combining the results of TG and EDS analysis, it can be inferred that the weight percentage of HA and Ag is 62.5 and 15.2 wt %, respectively. The tensile strength of Ag/HA and CS/Ag/HA coatings are 3.3 ± 1.1 MPa and 7.7 ± 2.0 MPa, respectively.

3.2. Ag Release and Antibacterial Activity of BMP/CS/Ag/HA Coatings. The release of Ag from BMP/CS/Ag/HA, CS/Ag/HA, and Ag/HA coatings exhibits sustained release kinetics without burst release. After 30 days of soaking in PBS, the total Ag ions that are released from BMP/CS/Ag/HA, CS/Ag/HA, and Ag/HA coatings are 4.7, 4.8, and 4.9 mg/L, respectively, which is high enough to inhibit bacterial growth (Figure 5a).[25,28] The Ag release rate of BMP/CS/Ag/HA coatings is comparable with that of CS/Ag/HA and Ag/HA coatings. To elaborate the mechanism for Ag and BMP release, the release profiles are fitted by typical drug release models. There are a series of widely used models, such as the zero order, first order, and Higuchi model. In this study, a simple Peppas model (eq 2) is selected to fit the release profiles:[30]

$$Q = kt^n \quad (2)$$

where Q is the fraction of total release, k is the kinetic constant, and n is the release exponent. In the thin film model, if $n < 0.5$, diffusion is Fickian; if $0.5 < n < 1$, diffusion is non-Fickian; and

dx.doi.org/10.1021/am501428e | ACS Appl. Mater. Interfaces 2014, 6, 8580−8589

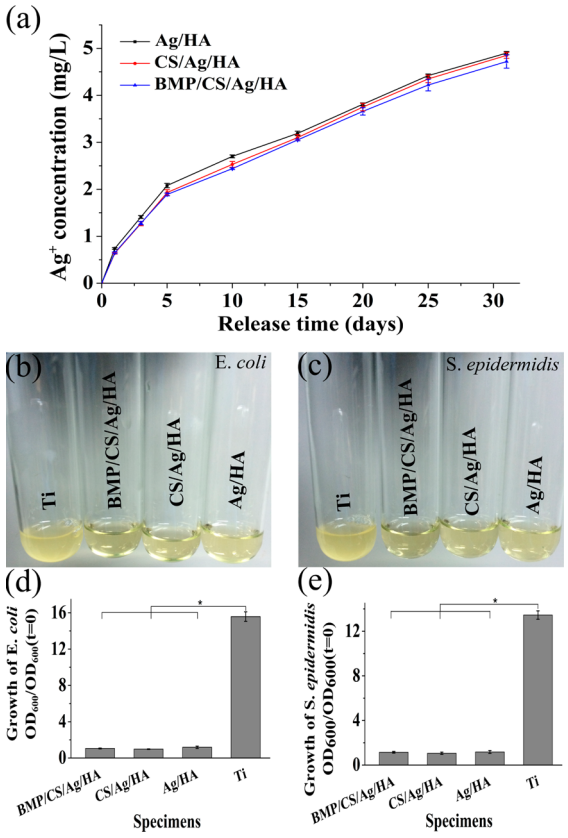

Figure 5. (a) In vitro release profiles of Ag ions from BMP/CS/Ag/HA, CS/Ag/HA, and Ag/HA coatings. (b) *E. coli* and (c) *S. epidermidis* suspensions that were cultured with different specimens for 24 h. Optical density measurement of growth of (d) *E. coli* and (e) *S. epidermidis* that were cultured with different specimens for 24 h.

if $n = 1$, zero order drug release mechanism dominates. The values of n of the Ag release profiles are shown in Table 1. The

Table 1. BMP Release Kinetics Parameters Obtained from the Peppas Model[a]

samples	k	n	r^2
BMP/CS/Ag/HA	11.58 ± 1.43	0.62 ± 0.06	0.984
BMP/Ag/HA	14.23 ± 0.64	0.69 ± 0.03	0.998

[a]The values are obtained when the released BMP is smaller than 60%.

values of n of three groups are in the range from 0.53 to 0.56, which reveals that Ag release is controlled by the non-Fickian diffusion mechanism that could be the combination of erosion and diffusion.

The BMP/CS/Ag/HA, CS/Ag/HA and Ag/HA coatings show strong antibacterial activities against both *E. coli* and *S. epidermidis*. As shown in Figure 5b and c, the color of the bacterial suspensions of BMP/CS/Ag/HA, CS/Ag/HA, and Ag/HA groups were clearer than that of pristine Ti after three groups were incubated with bacteria for 24 h, demonstrating that bacterial growth is inhibited on the BMP/CS/Ag/HA, CS/Ag/HA, and Ag/HA coatings. Quantitative analysis indicates that the bactericidal ratios of *E. coli* on Ag/HA, CS/Ag/HA, and BMP/CS/Ag/HA coatings are 93%, 94%, and 92%, respectively (Figure 5d). The bactericidal ratios of *S. epidermidis* on Ag/HA, CS/Ag/HA, and BMP/CS/Ag/HA coatings are 91%, 92%, and 91%, respectively (Figure 5e). These results indicate that the antibacterial activity of BMP/CS/Ag/HA and CS/Ag/HA is the same as the antibacterial activity of Ag/HA, and the addition of BMP/heparin and CS does not reduce the antibacterial activity of Ag in the coatings.

3.3. Biocompatibility of CS/Ag/HA Coatings. SEM images show that the CS/Ag/HA coatings favor osteoblast spreading and attachment (Figure 6a and e). The cell affinity of

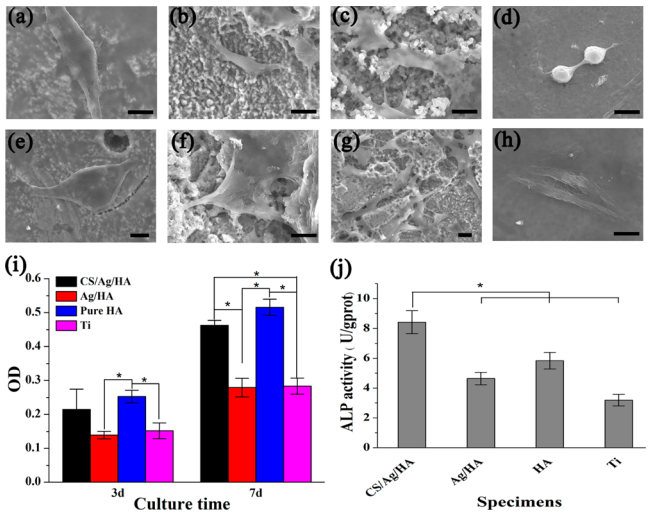

Figure 6. Morphologies, proliferation, and differentiation of OB on various coatings. (a) CS/Ag/HA coatings, 3 days. (b) Ag/HA coatings, 3 days. (c) Pure HA coatings, 3 days. (d) Pristine Ti, 3 days. (e) CS/Ag/HA coatings, 7 days. (f) Ag/HA coatings, 7 days. (g) Pure HA coatings, 7 days. (h) Pristine Ti, 7 days. (i) Proliferation of OB cells. (j) ALP activity of OB after 7 days culture. Scale bars: 10 μm. Asterisk (*) denotes significant differences ($p < 0.05$).

the CS/Ag/HA coatings could be partially attributed to the CS contained in the coatings. Cells also spread well on the Ag/HA (Figure 6b and f) and pure HA coatings (Figure 6c and g) because HA has the flowerlike structures in the coatings that could promote cell spreading and adhesion.[31] By contrast, cells on the pristine Ti surfaces spread well up to 7 days of culture (Figure 6d and h).

Results from Alamar Blue assay reveal that the proliferation of OB on CS/Ag/HA coatings is better than proliferation on Ag/HA coatings, and is comparable to proliferation on pure HA coatings (Figure 6i). After 3 days of culture, the proliferation activity of cells on CS/Ag/HA and Ag/HA coatings is lower than that on pure HA coatings and pristine Ti. After 7 days of culture, the proliferation activity of cells on CS/Ag/HA coatings is as high as that on pure HA coatings, and is significantly higher than that on Ag/HA coatings. Results from ALP activity test indicate that OB located on the CS/Ag/HA coatings have a significantly higher ALP activity than that on Ag/HA and pure HA coatings (Figure 6j). Comparison of osteoblast behaviors on CS/Ag/HA and Ag/HA coatings suggests that addition of CS reduces Ag toxicity in the coatings.

3.4. BMP-2 Release. Both BMP/CS/Ag/HA coatings and BMP/Ag/HA coatings exhibit sustained release kinetics. No burst release was observed in both groups. BMP-2 immobilized on CS/Ag/HA coatings has a slower release rate than when immobilized on Ag/HA coatings (Figure 7). Percentages of BMP-2 released from BMP/CS/Ag/HA and BMP/Ag/HA coatings after 25 days are approximately 56% and 86%, respectively. The release profiles of BMP were also fitted by the

dx.doi.org/10.1021/am501428e | ACS Appl. Mater. Interfaces 2014, 6, 8580−8589

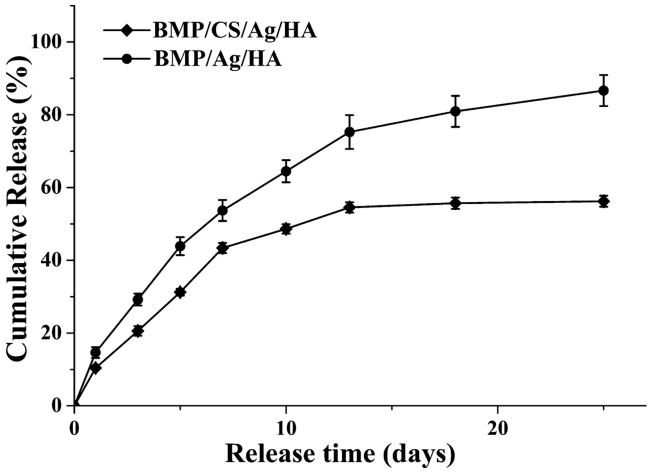

Figure 7. In vitro release profiles of BMP-2 from BMP/CS/Ag/HA and BMP/Ag/HA coatings.

Peppas model. The values of n are 0.62 and 0.69 (Table 2), respectively, which indicates that BMP release is dominated by a non-Fickian diffusion mechanism.

Table 2. Ag Release Kinetics Parameters Obtained from the Peppas Model[a]

samples	k	n	r^2
BMP/CS/Ag/HA	0.15 ± 0.02	0.54 ± 0.05	0.987
CS/Ag/HA	0.15 ± 0.02	0.56 ± 0.06	0.986
Ag/HA	0.17 ± 0.02	0.53 ± 0.05	0.988

[a]The values are obtained when the released Ag ions is smaller than 60%.

3.5. Culture of BMSCs. Immunofluorescence staining shows that BMSCs grow well on all groups (Figure 8a–j). Alamar Blue assay reveals that the proliferation of BMSCs on BMP/CS/Ag/HA coatings is nearly equal to that of BMSCs grown on CS/Ag/HA and pure HA coatings, and is higher than of BMSCs on BMP/Ag/HA coatings and pristine Ti (Figure 8k). ALP activity test showed that BMSCs on BMP/CS/Ag/HA coatings have higher ALP activity than other groups, which proves that BMSCs have been successfully induced to differentiate to osteoblasts by the BMP-2 released from BMP/CS/Ag/HA coatings (Figure 8l).

3.6. Histological Analysis. Histological analysis indicates that the BMP/CS/Ag/HA-Ti has high osteoconductivity in vivo. As shown in Figure 9, bone tissue is stained red by the Van Gieson's picro-fuchsine stain. The BMP/CS/Ag/HA-Ti is completely covered by bone tissue without a cartilaginous intermediate (Figure 9a). New bone grows outward from the implant surfaces and links with nearby host bone, which reveals the strong osteoconductivity of BMP/CS/Ag/HA-Ti. No significant Ag toxicity was found in the BMP/CS/Ag/HA-Ti group. In contrast, the BMP/Ag/HA-Ti was partly covered by bone tissue after 12 weeks implantation (Figure 9c). Osteocytes (marked by blue arrows) were also observed in the newly formed bone, which indicates bone maturation after 12 weeks implantation (Figure 9b and d).

3.7. Micro-CT Analysis. Micro-CT analysis proves strong osteoinductivity of BMP/CS/Ag/HA-Ti in vivo. Micro-CT slice imageing shows that new bone directly contacts with the surface of the implant, and the density of new bone is close to

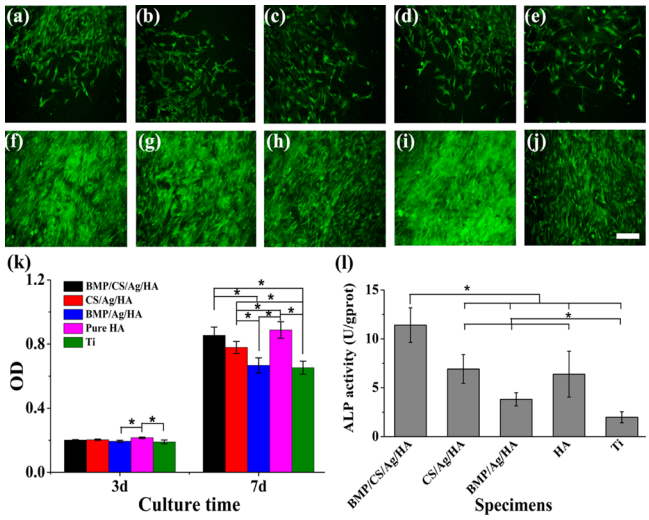

Figure 8. Immunofluorescence staining, proliferation, and differentiation of BMSCs on various coatings. (a) BMP/CS/Ag/HA coatings, 3 days. (b) CS/Ag/HA coatings, 3 days. (c) BMP/Ag/HA coatings, 3 days. (d) Pure HA coatings, 3 days. (e) Pristine Ti, 3 days. (f) BMP/CS/Ag/HA coatings, 7 days. (g) CS/Ag/HA coatings, 7 days. (h) BMP/Ag/HA coatings, 7 days. (i) Pure HA coatings, 7 days. (j) Pristine Ti. (k) Proliferation of BMSCs measured by Alamar Bule assay. (l) ALP activity of BMSCs after 14 days culture. Scale bars: 200 μm. Asterisk (*) denotes significant differences ($p < 0.05$).

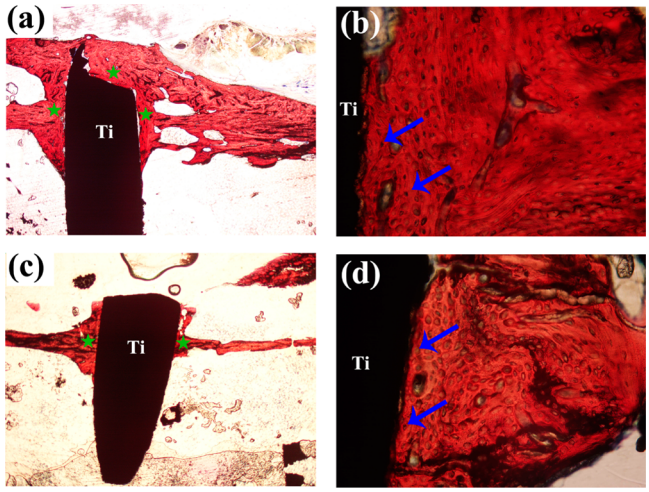

Figure 9. Histological sections of the implants stained with Van Gieson's picric acid-fuchsin after 12 weeks of implantation. (a) BMP/CS/Ag/HA-Ti. (b) Amplified image of (a). (c) BMP/Ag/HA-Ti. (d) Amplified image of (c). (a, c) Magnification ×16. (b, d) Magnification ×200. Green stars, new bone; blue arrows, osteocytes.

that of cortical bone (Supporting Information Figure S4a). Furthermore, Micro-CT 3D rendering images indicate that new bone also grows along the surface of the implant into the medullary cavity of the femur (Supporting Information Figure S4b and c).

4. DISCUSSION

Metallic implants require not only osteoinductivity that induces bone formation, but also antibacterial activity that protects the implants from contamination for long-term therapy.[32,33] Thus, the growth factors on implant surfaces for osteoinductivity and agents for antibacterial activity should maintain their

effectiveness for a desired period. First, the release of growth factor, such as BMP, should keep 2−3 weeks to promote bone healing. Secondly, the antibacterial agents should remain at the implant site for a sufficient period of time (about 6 weeks) to allow new bone formation.[34] Although loading antibiotics on the implant surfaces is widely used to prevent bacterial infections, previous reports indicate that antibiotics release fast during the initial few days.[35,36] Ag could ensure the long-term antibacterial activity of implants during the period of new bone formation. Wu et al.[37] loaded Ag into porous nano-HA/titiania/polyamide66 scaffolds, and found that Ag ions sustained release over 25 days in different medium. Li et al.[38] deposited nano-titania/Ag coatings on Ti substrates, and their results showed that Ag ions sustained release over 28 days from the coatings. In the present study, BMP/CS/Ag/HA coatings that can dual release BMP-2 and Ag ions were prepared, and were found to induce new bone formation and inhibit bacterial growth. The BMP-2 in the coatings releases over 25 days, and Ag ions release for more than 30 days. The release time of Ag ions is enough to protect the implants from infection during new bone formation process. Thus, this dual functional coating controls the infection and promotes new bone formation on Ti implants.

In the CS/Ag/HA coatings, the uniform distribution of Ag NPs was facilitated by using CS as a stabilizing agent. Ag^+ is chelated by two amino groups of chitosan.[39,40] The stabilization of Ag nanoparticles by CS could be ascribed to the nuncleophilic character of CS, which chelates Ag by donating electrons.[41] The SEM image shows that Ag tends to agglomerate and form large clusters in Ag/HA composite coatings (Scheme 1b). During the deposition of Ag/HA coatings, HA is formed by the reaction between Ca^{2+}, $H_2PO_4^-$, and OH^-. The OH^- is produced by the electrolysis of H_2O. Note that the standard reduction potential of Ag^+ is +0.7996, which is higher than the standard reduction potential of the electrolysis of H_2O, which suggests that reduction and deposition of Ag is easier and faster than that of HA. Thus, without a stabilizing agent, larger Ag clusters are formed because of the faster deposition rate of Ag, as reported in previous studies.[42,43] In our previous study, uniform distribution of Ag NPs in CaP coatings was obtained when L-cysteine was used as the stabilizing agent.[27] In the present study, CS was used as the stabilizing agent. CS chelates Ag ions to form CS-Ag^+ complexes in the electrolyte. During the ED process, CS−Ag^+ complexes move to the cathode under the assistance of electropotential and deposit on Ti surfaces. Thus, the reduction of Ag ions on the surface of the Ti cathode is maintained at a mild speed. After reduction, the electrostatic repulsive force between CS molecules prevents the aggregation of Ag NPs. A uniform distribution of Ag NP in the coatings is obtained (Scheme 1). Meanwhile, the release kinetics of Ag ions from CS/Ag/HA and Ag/HA coatings were compared, and results demonstrate that CS does not affect the release of Ag ions from HA coatings (Figure 5a).

CS/Ag/HA coatings demonstrate high antibacterial activity to bacteria and low toxicity to cells. Antibacterial tests reveal that CS/Ag/HA coatings exhibit strong antibacterial activity (Figure 5). Note that the effective antibacterial concentration of Ag varies in a large range in the literature. Chung et al.[25] synthesized Ag/HA coatings using a sol-gel method and observed that inhibition of bacterial growth around the Ag/HA coatings when the concentration of Ag ions ranges from 100 to 1000 ppm. Lee and Murphy[28] prepared Ag-contained CaP coatings using a biomimetic method, and results from their antibacterial tests revealed that the Ag concentrations ranging from 0.2 to 0.5 μg/mL are enough to inhibit bacteria growth. It should be pointed out that high concentration of Ag could be toxic to cells and detrimental to the biocompatibility of CaP coatings.[24,29] In the present study, the concentration of Ag ions released from Ag/HA and CS/Ag/HA coatings at each time interval ranges from 0.13 to 0.12 mg/L. Even these low concentrations of Ag ions that released from the coatings exhibit toxicity to osteoblasts to a certain extent. As shown in Figure 6, cells on Ag/HA coatings exhibit lower proliferation and differentiation activity than that on pure HA coatings. However, Ag toxicity is reduced by the addition of CS. Results from Alamar Blue and ALP assay show that CS/Ag/HA coatings are more favorable for osteoblast proliferation and differentiation compared with Ag/HA coatings. One possible reason is that addition of CS leads to uniform distribution of Ag NP in the coatings and prevent the formation of larger Ag clusters, which reduces the toxicity of Ag ions. Note that bare Ag NPs could entry into the cells and influence cell viability.[44] After being chelated by CS, Ag NPs show less toxicity because they cannot be uptaken and internalized by cells, as claimed by Travan et al.[40] In their work, they used CS-derived polysaccharide to stabilize Ag NPs, and the composite does not show cytotoxic effect toward cells. Geiser et al.[45] also declared that CS immobilized Ag NPs could generate physical barriers to Ag NPs diffusion into cells. Another reason for the good biocompatibility of CS/Ag/HA coatings is that CS itself promotes cell proliferation and adhesion, as previously reported in a number of studies.[46−49]

It is interesting that the ALP activities of the CS/Ag/HA sample are better than those of the HA sample for both OB and BMSCs. Generally speaking, OB could express ALP without BMP. HA has been widely reported to promote the ALP activity of OB. Hao et al.[50] sputtered HA coatings on Ti plates and cultured OB on the HA-coated Ti plates, and found that the ALP activity of OB on HA-coated Ti plates is significantly higher than that on pure Ti plates. Kim et al.[51] prepared HA coatings on Ti surfaces by a sol−gel method, and showed that HA-coated Ti promotes the ALP activity of human osteosarcoma cells. Moreover, previous studies indicate that CS could also enhance ALP expression of OB. Gaharwar et al.[49] added CS to silicate cross-linked poly(ethylene oxide) to promote cellular activity, and found that CS increases the ALP activity of MC3T3-E1 cells. Lin et al.[52] covalently bonded CS, alginate-cross-linked CS, and percin-cross-linked CS to Ti-6Al-4V surfaces and indicated that CS-based polymer coatings lead to faster OB proliferation and higher ALP expression. Furthermore, CS/HA composites for good cell activity and bone regeneration have also been reported. Thien et al.[53] prepared CS nanofibers by an electrospinning technique and then treated with simulated body fluid to generate HA on the surface. In their in vitro test, rat osteosarcoma cells exhibit high ALP activity on the CS/HA composite nanofibers. Kong et al.[54] combined HA into CS scaffolds by an in situ method, and found that the cells on composite scaffolds showed high ALP activity. In this study, ALP activity of OB on the CS/Ag/HA sample are better than that of cells on the HA sample, which probably could be ascribed to the synergistic effects of both CS and HA, and further study is needed.

The BMP-2 was mixed with heparin to form complex so as to maintain the activity. Heparin is a polyanion that can enhance the force of electrostatic interaction between CS and BMP-

2.[55,56] In addition, heparin has high binding affinity to BMP-2 and can protect the activity of BMP-2.[57] Lee et al.[58] immobilized the BMP-2/heparin complex on the poly-L-lysine grafted Ti by electrostatic interactions, and the results revealed that the BMP-2/heparin complex increases the ALP activity of MG63 cells. Ishibe et al.[59] used heparin to maintain the activity of BMP-2 on apatite-coated Ti. Their in vivo studies showed that new bone is formed around the apatite-covered Ti coated with BMP-2/heparin. These reports have proved that heparin could effectively maintain the activity of BMP-2. Our study demonstrated that BMSCs on the BMP-2/CS/Ag/HA coatings have high ALP activity, which proved that activity of BMP-2 is maintained in vitro. Moreover, the results from animal experiments also indicated that BMP-2 on BMP-2/CS/Ag/HA coatings has good activity in vivo.

The BMP/CS/Ag/HA coatings allow the sustained release of BMP-2. The release rate of BMP-2 in CS/Ag/HA coatings is significantly lower than that of Ag/HA coatings. BMP-2 is immobilized on CS/Ag/HA coatings by electrostatic interaction between CS and BMP-2/heparin. The release test shows that BMP-2 only release 10% on the first day and 56% at 25 days from BMP/CS/Ag/HA coatings, which is comparable and considerably better than other reports. Macdonald et al.[60] loaded BMP-2 in polyelectrolyte multilayers using the self-assembling method, and 80% BMP-2 was released during the first 2 days. Kim et al.[61] loaded BMP-2 on implant surfaces using a chemical cross-linking reaction, and 69% BMP-2 was released on the first day. In summary, the current results suggest that electrostatic interaction in the BMP/heparin/CS system is strong enough to immobilize BMP-2 molecules and allow for the sustained release of BMP-2.

The in vitro and in vivo studies indicate that BMP/CS/Ag/HA coatings have good osteoinductivity. The ALP assay shows that BMSCs have been induced to osteoblasts after 14 days of culture on BMP/CS/Ag/HA coatings. Animal experiments indicate that osteoinductivity of BMP/CS/Ag/HA-Ti is higher than that of BMP/Ag/HA-Ti. There are several reports on the incorporated of BMP-2 in CaP coatings. Wu et al.[62] employed two methods to load BMP on polymer substrates: in one method, BMP-2 and CaP were codeposited on the substrates, and in the other method BMP-2 was directly adsorbed on polymer substrates. Their in vivo studies indicate that BMP-2 incorporated CaP coatings are more efficacious in inducing bone formation than directly-adsorbed BMP-2. Hunziker et al.[63] also employed the biomimetic method to prepare two samples, namely, BMP-2 incorporated into CaP coatings and BMP-2 adsorbed on the surfaces of CaP coatings. They found that CaP coatings incorporated with BMP-2 have better performance based on in vivo studies. Bae et al.[64] prepared BMP-2 nanocomplex by the ionic interaction between BMP-2 and chondroitin sulfate, and codeposited BMP-2 nanocomplex with CaP on Ti surfaces. Their results revealed that the osteogenic activity of osteoblast cells was highly upregulated by the BMP-2/CaP coatings. Results obtained from the present study are similar to these previous reports, and thereby further confirming that BMP-2 stably immobilized in CaP coatings greatly enhances the osteoinductivity of CaP coatings.

5. CONCLUSIONS

BMP-2 and nano-Ag contained HA coatings on Ti surfaces were prepared by combining electrochemical deposition of Ag and electrostatic immobilization of BMP-2. Chitosan (CS) was selected as the suitable stabilizing agent to realize the uniform distribution of Ag nanoparticles in the HA coatings. CS also reduces Ag toxicity while retaining its antibacterial activity. In addition, CS facilitates the immobilization of BMP through the electrostatic interaction between biomolecules, including CS, heparin, and BMP. All the processes are conducted at mild conditions that favor growth factor incorporation. Sustained release of BMP-2 and Ag ions from HA coatings was successfully demonstrated for a long period. These coatings exhibit high osteoinductivity and antibacterial properties as revealed by in vitro and in vivo studies. In summary, this study presents a convenient and effective method for the incorporation of growth factors and antibacterial agents into CaP coatings.

■ ASSOCIATED CONTENT

Supporting Information

Schematic drawing of the implants and their insertion sites; FTIR spectra of pure CS powers and CS/Ag/HA coatings; TG and DTG curves of the CS/Ag/HA coatings; Micro-CT images of BMP/CS/Ag/HA-Ti implanted in the femur after 12 weeks of implantation. This material is available free of charge via the Internet at http://pubs.acs.org.

■ AUTHOR INFORMATION

Corresponding Author

*Tel.: +86-28-87634023. Fax: +86-28-87601371. E-mail: luxiong_2004@163.com.

Notes

The authors declare no competing financial interest.

■ ACKNOWLEDGMENTS

This project was financially supported by 863 Program, NSFC (31070851, 51202152), Program for New Century Excellent Talents in University (NCET-10-0704), Sichuan Youth Science-Technology Foundation (2011JQ0010), The Engineering Research Center of Biomass Materials (SWUST), Ministry of Education (12zxbk06), and Construction Program for Innovative Research Team of University in Sichuan Province (14TD0050).

■ REFERENCES

(1) Alghamdi, H. S.; Bosco, R.; van den Beucken, J. J.; Walboomers, X. F.; Jansen, J. A. Osteogenicity of Titanium Implants Coated with Calcium Phosphate or Collagen Type-I in Osteoporotic Rats. *Biomaterials* **2013**, *34*, 3747−3757.

(2) Shadanbaz, S.; Dias, G. J. Calcium Phosphate Coatings on Magnesium Alloys for Biomedical Applications: a Review. *Acta Biomater.* **2012**, *8*, 20−30.

(3) Zimmerli, W. Prosthetic-Joint-Associated Infections. *Best Pract. Res., Clin. Rheumatol.* **2006**, *20*, 1045−1063.

(4) Bose, S.; Tarafder, S. Calcium Phosphate Ceramic Systems in Growth Factor and Drug Delivery for Bone Tissue Engineering: a Review. *Acta Biomater.* **2012**, *8*, 1401−1421.

(5) Chien, C. Y.; Tsai, W. B. Poly(dopamine)-Assisted Immobilization of Arg-Gly-Asp Peptides, Hydroxyapatite, and Bone Morphogenic Protein-2 on Titanium to Improve the Osteogenesis of Bone Marrow Stem Cells. *ACS Appl. Mater. Interfaces* **2013**, *5*, 6975−6983.

(6) Rosen, V. BMP2 Signaling in Bone Development and Repair. *Cytokine Growth Factor Rev.* **2009**, *20*, 475−480.

(7) Axelrad, T. W.; Einhorn, T. A. Bone Morphogenetic Proteins in Orthopaedic Surgery. *Cytokine Growth Factor Rev.* **2009**, *20*, 481−488.

(8) Lee, K.; Silva, E. A.; Mooney, D. J. Growth Factor Delivery-Based Tissue Engineering: General Approaches and a Review of Recent Developments. *J. R. Soc., Interface* **2011**, *8*, 153−170.

(9) Liu, Y.; de Groot, K.; Hunziker, E. B. BMP-2 Liberated From Biomimetic Implant Coatings Induces and Sustains Direct Ossification in an Ectopic Rat Model. *Bone* **2005**, *36*, 745−757.
(10) Majid, K.; Tseng, M. D.; Baker, K. C.; Reyes-Trocchia, A.; Herkowitz, H. N. Biomimetic Calcium Phosphate Coatings as Bone Morphogenetic Protein Delivery Systems in Spinal Fusion. *Spine J.* **2011**, *11*, 560−567.
(11) Schuessele, A.; Mayr, H.; Tessmar, J.; Goepferich, A. Enhanced Bone Morphogenetic Protein-2 Performance on Hydroxyapatite Ceramic Surfaces. *J. Biomed. Mater. Res., Part A* **2009**, *90*, 959−971.
(12) Wong, L. S.; Khan, F.; Micklefield, J. Selective Covalent Protein Immobilization: Strategies and Applications. *Chem. Rev.* **2009**, *109*, 4025−4053.
(13) Norowski, P. A.; Bumgardner, J. D. Biomaterial and Antibiotic Strategies for Peri-implantitis. *J. Biomed. Mater. Res., Part B* **2009**, *88B*, 530−543.
(14) Oosterbos, C. J. M.; Vogely, H. C.; Nijhof, M. W.; Fleer, A.; Verbout, A. J.; Tonino, A. J.; Dhert, W. J. A. Osseointegration of Hydroxyapatite-Coated and Noncoated Ti6Al4V Implants in the Presence of Local Infection: a Comparative Histomorphometrical Study in Rabbits. *J. Biomed. Mater. Res.* **2002**, *60*, 339−347.
(15) Frommelt, L. Principles of Systemic Antimicrobial Therapy in Foreign Material Associated Infection in Bone Tissue, with Special Focus on Periprosthetic Infection. *Injury* **2006**, *37*, 87−94.
(16) Pratten, J.; Nazhat, S. N.; Blaker, J. J.; Boccaccini, A. R. In Vitro Attachment of Staphylococcus Epidermidis to Surgical Sutures with and without Ag-Containing Bioactive Glass Coating. *J. Biomater. Appl.* **2004**, *19*, 47−57.
(17) Campoccia, D.; Montanaro, L.; Speziale, P.; Arciola, C. R. Antibiotic-loaded Biomaterials and the Risks for the Spread of Antibiotic Resistance Following Their Prophylactic and Therapeutic Clinical Use. *Biomaterials* **2010**, *31*, 6363−6377.
(18) Ip, M.; Lui, S. L.; Poon, V. K.; Lung, I.; Burd, A. Antimicrobial Activities of Silver Dressings: an in Vitro Comparison. *J. Med. Microbiol.* **2006**, *55*, 59−63.
(19) Chen, Y. K.; Zheng, X. B.; Xie, Y. T.; Ding, C. X.; Ruan, H. J.; Fan, C. Y. Anti-bacterial and Cytotoxic Properties of Plasma Sprayed Silver-containing HA Coatings. *J. Mater. Sci.: Mater. Med.* **2008**, *19*, 3603−3609.
(20) Roy, M.; Fielding, G. A.; Beyenal, H.; Bandyopadhyay, A.; Bose, S. Mechanical, in Vitro Antimicrobial, and Biological Properties of Plasma-sprayed Silver-doped Hydroxyapatite Coating. *ACS Appl. Mater. Interfaces* **2012**, *4*, 1341−1349.
(21) Bai, X. A.; More, K.; Rouleau, C. M.; Rabiei, A. Functionally Graded Hydroxyapatite Coatings Doped with Antibacterial Components. *Acta Biomater.* **2010**, *6*, 2264−2273.
(22) Chen, W.; Liu, Y.; Courtney, H. S.; Bettenga, M.; Agrawal, C. M.; Bumgardner, J. D.; Ong, J. L. In Vitro Anti-bacterial and Biological Properties of Magnetron Co-sputtered Silver-containing Hydroxyapatite Coating. *Biomaterials* **2006**, *27*, 5512−5517.
(23) Song, W. H.; Ryu, H. S.; Hong, S. H. Antibacterial Properties of Ag (or Pt)-containing Calcium Phosphate Coatings Formed by Micro-arc Oxidation. *J. Biomed. Mater. Res., Part A* **2009**, *88A*, 246−254.
(24) Chen, W.; Oh, S.; Ong, A. P.; Oh, N.; Liu, Y.; Courtney, H. S.; Appleford, M.; Ong, J. L. Antibacterial and Osteogenic Properties of Silver-containing Hydroxyapatite Coatings Produced Using a Sol Gel Process. *J. Biomed. Mater. Res., Part A* **2007**, *82A*, 899−906.
(25) Chung, R. J.; Hsieh, M. F.; Huang, C. W.; Perng, L. H.; Wen, H. W.; Chin, T. S. Antimicrobial Effects and Human Gingival Biocompatibility of Hydroxyapatite Sol-Gel Coatings. *J. Biomed. Mater. Res., Part B* **2006**, *76*, 169−178.
(26) Chen, Y. K.; Zheng, X. B.; Xie, Y. T.; Ji, H.; Ding, C. X.; Li, H. W.; Dai, K. R. Silver Release from Silver-containing Hydroxyapatite Coatings. *Surf. Coat. Technol.* **2010**, *205*, 1892−1896.
(27) Lu, X.; Zhang, B. L.; Wang, Y. B.; Zhou, X. L.; Weng, J.; Qu, S. X.; Feng, B.; Watari, F.; Ding, Y. H.; Leng, Y. Nano-Ag-loaded Hydroxyapatite Coatings on Titanium Surfaces by Electrochemical Deposition. *J. R. Soc., Interface* **2011**, *8*, 529−539.
(28) Lee, J. S.; Murphy, W. L. Functionalizing Calcium Phosphate Biomaterials with Antibacterial Silver Particles. *Adv. Mater.* **2013**, *25*, 1173−1179.
(29) Qu, J.; Lu, X.; Li, D.; Ding, Y.; Leng, Y.; Weng, J.; Qu, S.; Feng, B.; Watari, F. Silver/hydroxyapatite Composite Coatings on Porous Titanium Surfaces by Sol-Gel Method. *J. Biomed. Mater. Res., Part B* **2011**, *97*, 40−48.
(30) Ritger, P. L.; Peppas, N. A. A Simple Equation for Description of Solute Release I. Fickian and Non-fickian Release from Non-swellable Devices in the form of Slabs, Spheres, Cylinders or Discs. *J. Controlled Release* **1987**, *5*, 23−36.
(31) Guo, X.; Gough, J. E.; Xiao, P.; Liu, J.; Shen, Z. Fabrication of Nanostructured Hydroxyapatite and Analysis of Human Osteoblastic Cellular Response. *J. Biomed. Mater. Res., Part A* **2007**, *82*, 1022−1032.
(32) Guelcher, S. A.; Brown, K. V.; Li, B.; Guda, T.; Lee, B. H.; Wenke, J. C. Dual-Purpose Bone Grafts Improve Healing and Reduce Infection. *J. Orthop. Trauma* **2011**, *25*, 477−482.
(33) Stewart, R. L.; Cox, J. T.; Volgas, D.; Stannard, J.; Duffy, L.; Waites, K. B.; Chu, T. M. The Use of a Biodegradable, Load-Bearing Scaffold as a Carrier for Antibiotics in an Infected Open Fracture Model. *J. Orthop. Trauma* **2010**, *24*, 587−591.
(34) Wenke, J. C.; Guelcher, S. A. Dual Delivery of an Antibiotic and a Growth Factor Addresses both the Microbiological and Biological Challenges of Contaminated Bone Fractures. *Expert Opin. Drug Delivery* **2011**, *8*, 1555−1569.
(35) Li, L. L.; Wang, L. M.; Xu, Y.; Lv, L. X. Preparation of Gentamicin-loaded Electrospun Coating on Ttanium Implants and a Study of Their Properties in Vitro. *Arch. Orthop. Trauma Surg.* **2012**, *132*, 897−903.
(36) Tu, J.; Yu, M.; Lu, Y.; Cheng, K.; Weng, W.; Lin, J.; Wang, H.; Du, P.; Han, G. Preparation and Antibiotic Drug Release of Mineralized Collagen Coatings on Titanium. *J. Mater. Sci. Mater. Med.* **2012**, *23*, 2413−2423.
(37) Wu, X.; Li, J.; Wang, L.; Huang, D.; Zuo, Y.; Li, Y. The Release Properties of Silver Ions from Ag-nHA/TiO_2/PA66 Antimicrobial Composite Scaffolds. *Biomed. Mater.* **2010**, *5*, 044105.
(38) Li, B.; Liu, X.; Meng, F.; Chang, J.; Ding, C. Preparation and Antibacterial Properties of Plasma Sprayed Nano-titania/silver Coatings. *Mater. Chem. Phys.* **2009**, *118*, 99−104.
(39) Katarina, R. K.; Takayanagi, T.; Oshima, M.; Motomizu, S. Synthesis of a Chitosan-based Chelating Resin and its Application to the Selective Concentration and Ultratrace Determination of Silver in Environmental Water Samples. *Anal. Chim. Acta* **2006**, *558*, 246−253.
(40) Travan, A.; Pelillo, C.; Donati, I.; Marsich, E.; Benincasa, M.; Scarpa, T.; Semeraro, S.; Turco, G.; Gennaro, R.; Paoletti, S. Non-cytotoxic Silver Nanoparticle-polysaccharide Nanocomposites with Antimicrobial Activity. *Biomacromolecules* **2009**, *10*, 1429−1435.
(41) Henglein, A. Physicochemical Properties of Small Metal Particles in Solution - Microelectrode Reactions, Chemisorption, Composite Metal Particles, and the Atom-to-Metal Transition. *J. Phys. Chem.* **1993**, *97*, 5457−5471.
(42) Rezaei, B.; Damiri, S. Electrodeposited Silver Nanodendrites Electrode With Strongly Enhanced Electrocatalytic Activity. *Talanta* **2010**, *83*, 197−204.
(43) Chen, Y. P.; Zhao, Y.; Qiu, K. Q.; Chu, J.; Yu, H. Q.; Liu, G.; Tian, Y. C.; Xiong, Y. Fabrication of Dendritic Silver Nanostructure Using an Integration of Holographic Lithography and Electrochemical Deposition. *Electrochim. Acta* **2011**, *56*, 9088−9094.
(44) AshaRani, P. V.; Low Kah Mun, G.; Hande, M. P.; Valiyaveettil, S. Cytotoxicity and Genotoxicity of Silver Nanoparticles in Human Cells. *ACS Nano* **2008**, *3*, 279−290.
(45) Geiser, M.; Rothen-Rutishauser, B.; Kapp, N.; Schurch, S.; Kreyling, W.; Schulz, H.; Semmler, M.; Im Hof, V.; Heyder, J.; Gehr, P. Ultrafine Particles Cross Cellular Membranes by Nonphagocytic Mechanisms in Lungs and in Cultured Cells. *Environ. Health Perspect.* **2005**, *113*, 1555−1560.
(46) Chua, P. H.; Neoh, K. G.; Kang, E. T.; Wang, W. Surface Functionalization of Titanium with Hyaluronic Acid/chitosan Polyelectrolyte Multilayers and RGD for Promoting Osteoblast

Functions and Inhibiting Bacterial Adhesion. *Biomaterials* **2008**, *29*, 1412−1421.
(47) Freier, T.; Koh, H. S.; Kazazian, K.; Shoichet, M. S. Controlling Cell Adhesion and Degradation of Chitosan Films by N-acetylation. *Biomaterials* **2005**, *26*, 5872−5878.
(48) Di Martino, A.; Sittinger, M.; Risbud, M. V. Chitosan: A Versatile Biopolymer for Orthopaedic Tissue-engineering. *Biomaterials* **2005**, *26*, 5983−5990.
(49) Gaharwar, A. K.; Schexnailder, P. J.; Jin, Q.; Wu, C. J.; Schmidt, G. Addition of Chitosan to Silicate Cross-linked PEO for Tuning Osteoblast Cell Adhesion and Mineralization. *ACS Appl. Mater. Interfaces* **2010**, *2*, 3119−3127.
(50) Hao, J.; Kuroda, S.; Ohya, K.; Bartakova, S.; Aoki, H.; Kasugai, S. Enhanced Osteoblast and Osteoclast Responses to a Thin Film Sputtered Hydroxyapatite Coating. *J. Mater. Sci.: Mater. Med.* **2011**, *22*, 1489−1499.
(51) Kim, H. W.; Kim, H. E.; Salih, V.; Knowles, J. C. Sol-Gel-modified Titanium With Hydroxyapatite Thin Films and Effect on Osteoblast-like Cell Responses. *J. Biomed. Mater. Res., Part A* **2005**, *74*, 294−305.
(52) Lin, H. Y.; Chen, J. H. Osteoblast Differentiation and Phenotype Expressions on Chitosan-coated Ti-6Al-4V. *Carbohydr. Polym.* **2013**, *97*, 618−626.
(53) Thien, D. H.; Hsiao, S. W.; Ho, M. H.; Li, C. H.; Shih, J. L. Electrospun Chitosan/hydroxyapatite Nanofibers for Bone Tissue Engineering. *J. Mater. Sci.* **2012**, *48*, 1640−1645.
(54) Kong, L.; Gao, Y.; Lu, G.; Gong, Y.; Zhao, N.; Zhang, X. A Study on the Bioactivity of Chitosan/nano-hydroxyapatite Composite Scaffolds for Bone Tissue Engineering. *Eur. Polym. J.* **2006**, *42*, 3171−3179.
(55) Ruppert, R.; Hoffmann, E.; Sebald, W. Human Bone Morphogenetic Protein 2 Contains a Heparin-binding Site which Modifies Its Biological Activity. *Eur. J. Biochem.* **1996**, *237*, 295−302.
(56) Bhakta, G.; Rai, B.; Lim, Z. X. H.; Hui, J. H.; Stein, G. S.; van Wijnen, A. J.; Nurcombe, V.; Prestwich, G. D.; Cool, S. M. Hyaluronic Acid-based Hydrogels Functionalized with Heparin that Support Controlled Release of Bioactive BMP-2. *Biomaterials* **2012**, *33*, 6113−6122.
(57) Gandhi, N. S.; Mancera, R. L. Prediction of heparin binding sites in bone morphogenetic proteins (BMPs). *Biochim. Biophys. Acta, Proteins Proteomics* **2012**, *1824*, 1374−1381.
(58) Lee, S. Y.; Yun, Y. P.; Song, H. R.; Chun, H. J.; Yang, D. H.; Park, K.; Kim, S. E. The Effect of Titanium with Heparin/BMP-2 Complex for Improving Osteoblast Activity. *Carbohydr. Polym.* **2013**, *98*, 546−554.
(59) Ishibe, T.; Goto, T.; Kodama, T.; Miyazaki, T.; Kobayashi, S.; Takahashi, T. Bone Formation on Apatite-coated Titanium with Incorporated BMP-2/heparin in Vivo. *Oral Surg., Oral Med., Oral Pathol., Oral Radiol. Endodontol.* **2009**, *108*, 867−875.
(60) Macdonald, M. L.; Samuel, R. E.; Shah, N. J.; Padera, R. F.; Beben, Y. M.; Hammond, P. T. Tissue Integration of Growth Factor-eluting Layer-by-layer Polyelectrolyte Multilayer Coated Implants. *Biomaterials* **2011**, *32*, 1446−1453.
(61) Kim, S. E.; Song, S. H.; Yun, Y. P.; Choi, B. J.; Kwon, I. K.; Bae, M. S.; Moon, H. J.; Kwon, Y. D. The Effect of Immobilization of Heparin and Bone Morphogenic protein-2 (BMP-2) to Titanium Surfaces on Inflammation and Osteoblast Function. *Biomaterials* **2011**, *32*, 366−373.
(62) Wu, G.; Liu, Y.; Iizuka, T.; Hunziker, E. B. The Effect of a Slow Mode of BMP-2 Delivery on the Inflammatory Response Provoked by Bone-defect-filling Polymeric Scaffolds. *Biomaterials* **2010**, *31*, 7485−7493.
(63) Hunziker, E. B.; Enggist, L.; Kuffer, A.; Buser, D.; Liu, Y. Osseointegration: The Slow Delivery of BMP-2 Enhances Osteoinductivity. *Bone* **2012**, *51*, 98−106.
(64) Bae, S. E.; Choi, J.; Joung, Y. K.; Park, K.; Han, D. K. Controlled Release of Bone Morphogenetic Protein (BMP)-2 from Nanocomplex Incorporated on Hydroxyapatite-formed Titanium Surface. *J. Controlled Release* **2012**, *160*, 676−684.